

A new inclination instability reshapes Keplerian disks into cones: application to the outer Solar System

Ann-Marie Madigan^{1*} and Michael McCourt²

¹ *Astronomy Department and Theoretical Astrophysics Center, University of California, Berkeley, CA 94720, USA*

² *Institute for Theory and Computation, Harvard University, Center for Astrophysics, 60 Garden St., Cambridge, MA 02138*

1 October 2015

ABSTRACT

Disks of bodies orbiting a much more massive central object are extremely common in astrophysics. When the orbits comprising such disks are eccentric, we show they are susceptible to a new dynamical instability. Gravitational forces between bodies in the disk drive exponential growth of their orbital inclinations and clustering in their angles of pericenter, expanding an initially thin disk into a conical shape by giving each orbit an identical “tilt” with respect to the disk plane. This new instability dynamically produces the unusual distribution of orbits observed for minor planets beyond Neptune, suggesting that the instability has shaped the outer Solar System. It also implies a large initial disk mass ($\sim 1 - 10$ Earth masses) of scattered bodies at hundreds of AU; we predict increasing numbers of detections of minor planets clustered in their angles of pericenter with high inclinations.

Key words: celestial mechanics — planets and satellites: dynamical evolution and stability — minor planets — stars: kinematics and dynamics

1 INTRODUCTION

Disks of bodies orbiting a more massive central object are ubiquitous in the universe: examples include moons around a planet, planets around a star, or stars around a super-massive black hole. The long-lived, periodic interactions among closed orbits in these disks can drive rapid angular momentum evolution among bodies comprising the disk (e.g., “resonant-relaxation” of stars near massive black holes; Rauch & Tremaine 1996) and collective behavior such as spontaneous organization or dynamical instability (Madigan, Levin & Hopman 2009). While particles in circular disks do not undergo collective behavior and are understood to diffuse slowly in inclination only through two-body scattering (Ida 1990), we show here that disks of particles with high eccentricity orbits instead collect in angle of pericenter and undergo exponential growth in inclination; we refer to this new process as the *inclination instability*.

In this letter, we demonstrate the inclination instability and illustrate its essential characteristics; we also present evidence that the outer Solar System has undergone the inclination instability, and that it reproduces the bizarre and unexplained distribution of orbits of minor planets beyond Neptune. We describe the secular dynamical mechanism by which the instability works in a forthcoming paper (Madigan & McCourt, *in prep.*).

2 THE INCLINATION INSTABILITY

In order to demonstrate the inclination instability, we consider a thin, axisymmetric disk of particles on eccentric orbits around a much more massive central object. Two angles are required to orient an orbital plane in space;¹ we adopt two inclination angles i_a and i_b . These angles represent rotations of the orbit with normal vector \hat{j} about its semi-major (\hat{a}) axis and its semi-minor ($\hat{b} \equiv \hat{j} \times \hat{a}$) axis, respectively:

$$\tan(i_a) = \frac{\hat{b}_z}{\sqrt{1 - \hat{b}_z^2}} \quad (1a)$$

$$\tan(i_b) = -\frac{\hat{a}_z}{\sqrt{1 - \hat{a}_z^2}} \quad (1b)$$

Though non-standard, the angles i_a and i_b are characteristic coordinates of the inclination instability and greatly simplify our analysis.

Figure 1 shows the evolution of the inclination angles i_a and i_b in an N -body simulation of low-mass bodies orbiting a central object of mass M . We initialize $N = 100$ particles in an axisymmetric disk with a total mass $M_{\text{disk}} = 10^{-4}M$ and identical eccentricities $e=0.9$. We perform integrations using the *mercury6* code (Chambers 1999). We normalize time to the secular dynamical timescale $t_{\text{sec}} \equiv (M/M_{\text{disk}})P$, where P is a typical orbital period. The top panel of figure 1 shows that the inclination angles initially grow

* ann-marie@astro.berkeley.edu

¹ Traditionally the longitude of ascending node Ω and inclination angle i .

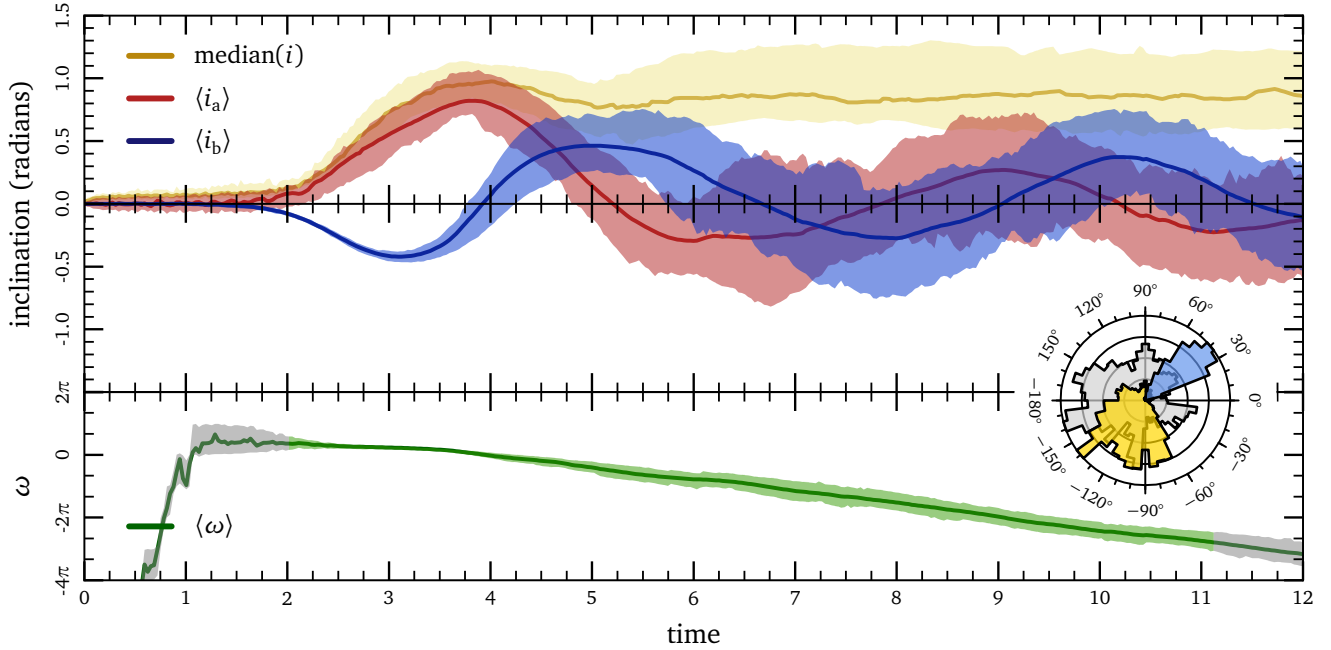


Figure 1. (top): Evolution of the inclination angles i_a and i_b (defined in equation 1) for particles initially forming a thin, near-Keplerian disk. Lines show median/mean angles and the shaded region encloses the 25th and 75th quantiles, i.e. enclosing 50% of the particles. Orbital inclinations initially grow rapidly due to the inclination instability. Each orbit has approximately the same inclination, with i_a and i_b initially growing together in a fixed ratio < 0 . After the instability saturates around a time $t \sim 3$, the orbits precess coherently about the mean angular momentum axis of the disk. (bottom): Evolution of the angle of pericenter ω . The inclination instability causes the orbits to collapse into a narrow distribution of ω around a time $t \sim 2-3$. This clustering in ω is not actively maintained after the instability saturates, and spreads due to differential precession by a time $t \sim 6.5$. As in the top panel, the colored region shows the width of the distribution enclosing half of the orbits. We mark this as green where the width is less than $\pm 55^\circ$, the observed scatter for minor planets beyond Neptune (see section 3, below). (inset): angular distribution of ω during the linear, exponentially growing phase from $t \sim 2.5-3$ (blue) and in the saturated state ($t \sim 5.5-6$; yellow). The asymmetry in ω persists even at late times ($t \sim 11.5-12$; gray).

rapidly, with opposite signs $i_b/i_a < 0$ and with $|i_a| < |i_b|$. All three of these features are inconsistent with known processes such as scattering or resonant relaxation; to our knowledge, this behavior is uniquely characteristic of the inclination instability.

The instability saturates, and exponential growth of orbital inclination halts, when inclinations reach ~ 1 radian. After this time, we see large-scale, coherent precession of the orbits' individual angular momentum vectors about the mean angular momentum of the disk; this large-scale precession produces the slow oscillations in i_a and i_b seen at late times in figure 1, while preserving the overall inclinations of the orbits [$i \equiv \arccos(j_z/j)$].

A direct observational signature of the inclination instability is the distribution of orbits in angle of pericenter² ω : The bottom panel of figure 1 shows that, during the exponentially growing phase of the instability, this distribution of ω values collapses to an extremely narrow range $\omega \sim (45 \pm 15)^\circ$. The distribution remains narrow even after the exponential phase of the instability ends, though it eventually spreads out due to differential axial precession of orbits within the disk. Physically, a tight distribution in ω implies that orbits tilt uniformly out of the disk plane, giving the disk a conical shape; see figure 4 for a 3D visualization. The top panel of figure 1 shows that the inclination instability creates this shape by simultaneously giving each orbit similar values for i_a and i_b . This

tilt moves the center of mass of the disk off the original disk plane and drives the late-time precession seen in the top panel of figure 1.

The bottom panel of figure 1 shows that the inclination instability drives ω to a constant value $\sim 45^\circ$ during its linear, exponentially-growing phase from $t \sim 1$ until $t \sim 3$ ish. Before this time, orbits individually undergo retrograde axial precession.³ This axial precession is driven by self-gravity of the disk, which introduces a non-keplerian force on particles toward the disk plane; consequently, ω increases roughly linearly with time before the instability sets in. After the inclination instability collects orbits in angle of pericenter (effectively rearranging the disk into a conical shape), the dominant non-keplerian force no longer points toward the disk plane, but instead toward the disk's axis of symmetry, above or below the disk plane. This force drives *prograde* axial precession, reversing the trend in ω as seen in figure 1 after $t \sim 3$ ish.

Figure 2 further quantifies the development of the inclination instability. The top panel shows the inclination angles i_a and i_b as functions of time during the linear phase of the instability, clearly demonstrating the exponential growth expected for a true dynamical instability. At early times in the simulation, the angular momentum vectors precess rapidly and incoherently about the mean angular momentum of the disk; this precession represents oscillations in i_a and i_b with $|i_a| > |i_b|$, and it dominates the orbital inclinations until the inclination instability takes over around a time $t \sim 1-1.5$.

² $\omega = \arccos \hat{n} \cdot \hat{e}$, is the angle between the vector of ascending node and eccentricity vector.

³ while the orbits also undergo apsidal precession, the rate of this precession is much lower for the high eccentricities considered here.

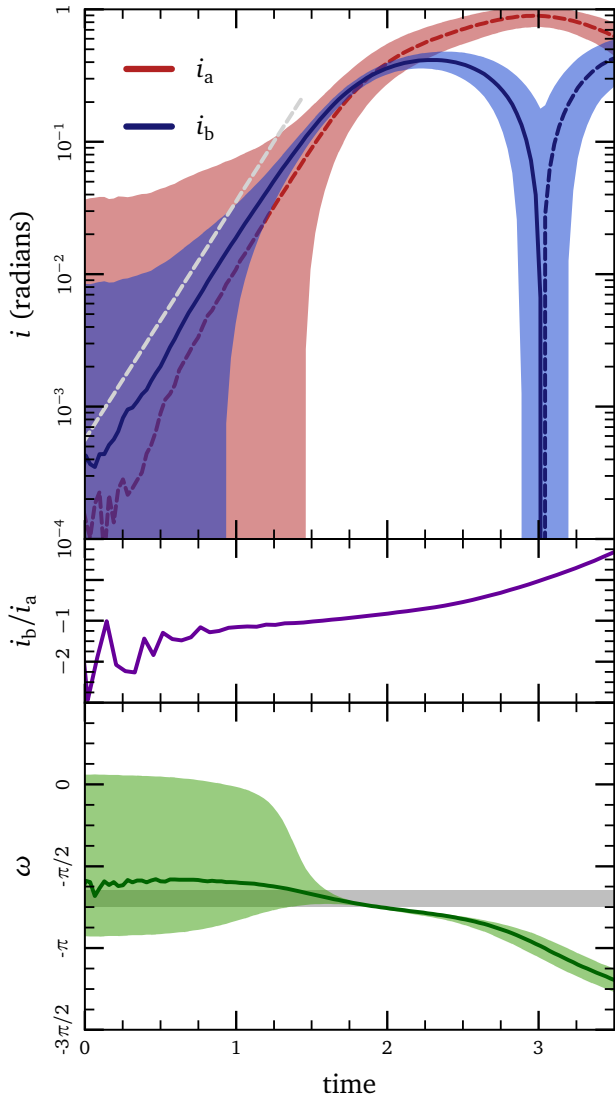


Figure 2. Quantitative evolution of the inclination instability. (*top*): Exponential growth of the inclination angles i_a and i_b . Lines show the median values of all the orbits and the colored bands show the width of the distribution enclosing 50% of the orbits. Solid lines indicate positive values, and dashed lines indicate negative values. At early times, the individual angular momentum vectors precess incoherently; this precession implies oscillations in i_a and i_b with $|i_a| > |i_b|$. The precession averages to zero upon taking the median, revealing exponential growth with $|i_b| > |i_a|$. The instability is present even at low inclinations ($< 1^\circ$) though this may not be observable in systems of small numbers of bodies. (*middle*): Evolution of the ratio $\langle i_b \rangle / \langle i_a \rangle$. Though $\langle i_b \rangle$ and $\langle i_a \rangle$ individually grow by more than two orders of magnitude from $t \sim 0-1.5$, their ratio remains constant to within a factor of 2. (*bottom*): Evolution in mean angle of pericenter. We over-plot a theoretical prediction. The colored bands show the width of the distribution enclosing 50% of the orbits. The distribution in ω remains tight even after the exponential growth phase ends.

The colored bands in the top panel of figure 2 indicate the width of the distribution by enclosing 50% of the orbits; this indicates the amplitude of the precession. The initial precession is incoherent, however, and its effects average away upon taking the median. The thick curves in the top panel of figure 2 thus reveal exponential growth with $|i_b| > |i_a|$ even at early times $t < 1$, when the instability is much lower in amplitude than the precession. (We include the

results of 1024 independent simulations to reduce the noise in this average).

The physical mechanism behind the inclination instability implies a constant (but eccentricity-dependent) ratio $i_b/i_a \lesssim -1$ (Madigan & McCourt, *in prep.*). The two curves in the top panel of figure 2 show i_a and i_b growing at a constant, negative ratio at early times. We demonstrate this explicitly in the middle panel, where we plot the ratio $\langle i_b \rangle / \langle i_a \rangle$; though the curve is noisy due to precession (larger in magnitude by a factor of ~ 100), this ratio is consistent with the theoretical model. Though $\langle i_b \rangle$ and $\langle i_a \rangle$ individually grow by more than two orders of magnitude during the linear, exponentially-growing phase of the instability, their ratio remains constant to within a factor of 2.

For small inclinations, a constant ratio i_b/i_a implies a constant angle of pericenter $\omega \sim \arctan(|i_b/i_a|)$ ($+\pi$ if $i_a < 0$). The bottom panel of figure 2 shows the angle of pericenter ω as a function of time in our simulation, along with our theoretical expectation (Madigan & McCourt *in prep.*). As in the top panel, the colored region encloses 50% of the orbits and quantifies the scatter in the simulation. Individual orbital precession dominates the inclinations until a time $t \sim 1$ and leads to a large scatter of $\sim 2\pi$; however, the distribution tightens considerably once the inclination instability dominates the dynamics. As seen in figure 1, the distribution remains narrow even after the exponential phase of the instability ends around the time $t \sim 2$.

Figure 4 shows the geometric meaning of this narrow distribution in ω . The middle and bottom panels show two disks in which every orbit has the same semi-major axis a , eccentricity $e = 0.8$, and inclination $i = 0.5$. In the middle panel, every orbit has the same value of $\omega = -1$; the orbits in this disk coherently tilt above the disk plane to form a cone shape. (For positive values of ω , the orbits would tilt below the plane.) In the bottom panel, we give each orbit a random value of ω ; this disk thickens isotropically into a torus.

3 DISCUSSION

The tight distribution in ω (or corresponding conical shape to the disk) is a unique observational signature of the inclination instability. Trujillo & Sheppard (2014) report such a signature in observations of minor planets beyond Neptune ($a = 30$ AU). These icy bodies are hypothesized to have formed much closer to the sun, scattering off Neptune to distant, high eccentricity orbits during the migration phase of the gas- and ice-giants (Tsiganis et al. 2005). Trujillo and Sheppard show that the angles of pericenter for minor planets with semi-major axes $a > 150$ AU and pericenter distances $r_{\text{peri}} > 30$ AU cluster about $\langle \omega \rangle = (340 \pm 55)^\circ$ (see the top panel of figure 4). This clustering cannot be explained by any known observational biases. The authors suggest that a stochastic event, such as a strong stellar encounter early in the Solar System’s evolution, could produce an initially asymmetric population in ω . To prevent ω values from subsequently randomizing, they invoke a massive unseen perturber, such as a trans-Plutonian super-Earth at $a \sim 250$ AU.

We propose a simpler solution: the minor planets underwent the inclination instability $\sim 1-4$ Gyr ago, exponentially growing in inclination, and developing a narrow distribution in ω centered on 45° (for very eccentric orbits) to $\sim 70^\circ$ (for lower eccentricity). Afterwards, the distribution of ω values drifted clockwise and

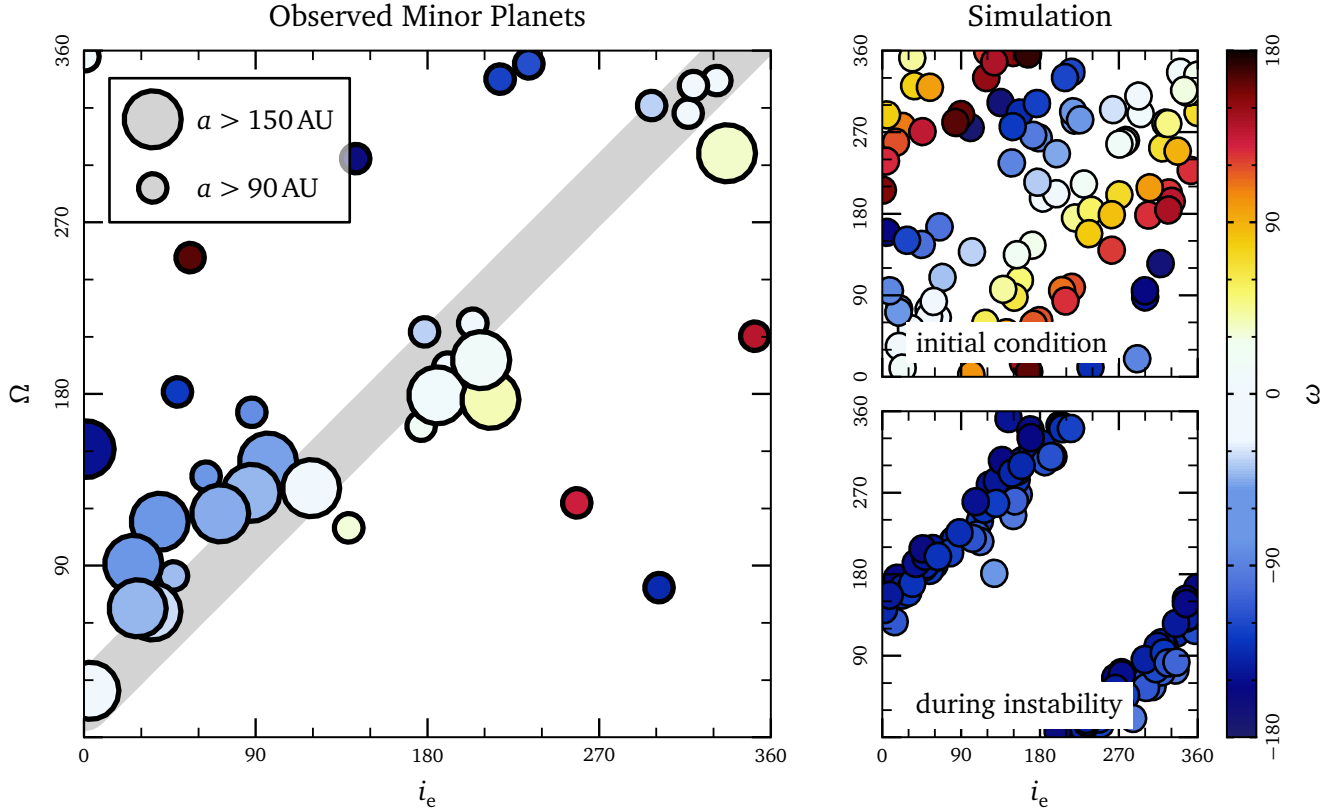


Figure 3. Inclination instability in the outer Solar System. (*left*): orientation angles measured for minor planets in the solar system. We show all known minor planets with pericenter distances greater than Neptune’s orbit (30 AU) and with semi-major axes greater than 90 AU (small circles) and 150 AU (large circles, cf. Trujillo & Sheppard (2014)). We plot the longitude of ascending node Ω and the angle $i_e \equiv \arctan(a_y, a_x)$, which represents the orientation of the semi-major axis (or eccentricity vector) within the reference plane. Orbits randomly distributed within a disk would fill out this space, however the minor planets only occupy a narrow band. Error bars are smaller than symbols. (*right*): N -body simulation of the inclination instability in a disk with 100 particles and a total mass $M_{\text{disk}} = 10^{-4} M$. The top panel shows the initial condition for the simulation; orbits randomly distributed within the disk populate the entire $\Omega-i_e$ space. During the inclination instability, this distribution collapses to a narrow band in $\Omega-i_e$ space, as is seen in the outer solar system. In all plots, color indicates the angle of pericenter ω ; banding in $\Omega-i_e$ space corresponds to clustering in ω .

widened due to precession, before reaching the current value of $\langle \omega \rangle = (-20 \pm 55)^\circ$.⁴

Clustering in ω implies a tight correlation between the angle of ascending node Ω and i_e , the orientation of the semi-major axis (or eccentricity vector) as projected in the initial disk plane; i. e., $i_e \equiv \arctan(a_y, a_x)$. We show this in figure 3, where we compare observational data with results from our N -body simulations. In the left panel, we plot the observed $\Omega-i_e$ distribution for minor planets, with the gray line corresponding to a constant $\omega = 340^\circ$. Data is taken from the IAU Minor Planet Center.⁵ We select minor planets with $r_{\text{peri}} > 30$ AU and $a > 150$ AU, as in Trujillo & Sheppard (2014). In order to show that this clustering is not an artifact of any particular cut to the data, we also plot all minor planets with $a > 90$ AU. Orbits randomly placed within a disk would populate this entire plot; however the minor planets show a clear correlation between Ω and i_e .

In the right panels of figure 3, we plot the $\Omega-i_e$ distribution for an N -body simulation in the initial condition (*top*) and during

the inclination instability (at time $t \sim 1$; *bottom*). At early times, bodies in the disk fill out the entire $\Omega-i_e$ space. During the instability, however, the distribution collapses to a thin band, with a shape and thickness that resembles the minor planet data. After the exponential phase ends, the band sweeps slowly across the plot as ω values drift due to large-scale precession. The green shaded region in the bottom panel of figure 1 shows the time during which the ω values lie within the scatter observed for minor planets in our solar system; the distribution in ω remains tight for another ~ 10 secular timescales after the instability saturates. This length of time is likely to be far longer than the age of the Solar System (however, this timescale may be shortened by perturbations from the gas giants or from the galactic tidal field, not included here).

In addition to explaining the clustering of minor planets in argument of pericenter, the inclination instability furthermore reproduces the high orbital inclinations of minor planets with respect to the ecliptic [$i \sim (5 - 30)^\circ$]. Even more suggestive is the paucity of planets with low inclinations; this cannot be understood as the result of scattering, but is a natural outcome of the inclination instability. The top panel of figure 1 shows that inclinations remain high for long periods of time, possibly indefinitely, after being pumped by the instability.

The inclination instability also provides a natural explanation

⁴ Depending on the precession rate and the time since the instability, both of which depend on the unknown mass of the disk, $\langle \omega \rangle$ could equally have begun between -45° and 0° , drifting through $\sim 2\pi$ to reach its current state.

⁵ <http://www.minorplanetcenter.net>

for “detached” minor planets, which have pericenter distances larger (by $\geq 25\%$) than Neptune’s orbit (Gladman et al. 2002; Lorenzo 2007). Since the effectiveness of gravitational scattering from the gas and ice giants strongly decreases for pericenter distances above 35 AU (Duncan, Quinn & Tremaine 1987), detached objects cannot be explained through scattering. However, detachment is a natural outcome of the inclination instability: as orbital inclinations grow, eccentricities drop due to conservation of angular momentum, and pericenter distances [$\propto (1 - e)$] thus increase beyond the reach of the giant planets in the inner Solar System. We study the detailed interaction between scattering and the inclination instability early in this detachment process in an upcoming paper (Madigan, *in prep.*).

The inclination instability naturally explains the clustering in ω of the minor planets beyond Neptune, and the corresponding correlation in $\Omega - i_e$ space, the high orbital inclinations of these objects, and the population of detached minor planets. Thus, *the inclination instability qualitatively reproduces the distribution of minor planet orbits, beginning from a generic initial condition.* This scenario implies an initial total disk mass of $\sim 1 - 10$ Earth masses distributed between ~ 50 AU and $\sim 10^4$ AU, at least an order of magnitude larger than the estimated current mass in the Kuiper Belt at smaller radii ($a \sim 30 - 50$ AU) (Gladman et al. 2001).

Existing simulations of the formation of the outer Solar System predict very few minor planets at distances between ~ 50 AU and $\sim 10^4$ AU (Duncan, Quinn & Tremaine 1987). However, there are few observational constraints on this region, as it is an empty loss-cone regime (Hills 1981). Moreover, in recent years, nearly two hundred minor planets have been discovered with semi-major axes of hundreds of AU, despite the extreme difficulty of finding such objects. It thus seems entirely possible that earlier theoretical predictions are incorrect, and that a massive reservoir of minor planets exists beyond the Kuiper Belt. We predict increasing numbers of detections of minor planets clustered in $\omega \sim (-20 \pm 55)^\circ$ values, with high inclinations and semi-major axes of ~ 100 s of AU. A further prediction of the inclination instability is that $d\langle\omega\rangle/da > 0$; that is, mean ω values of minor planets should increase with semi-major axis. In an upcoming paper, we make more specific, statistical predictions for where new minor planets should be found.

We close by noting that the inclination instability also has implications for the dynamics of stars orbiting super-massive black holes in galactic nuclei. For example, the disk of young stars in our Galactic center is much thicker than can be understood via scattering or resonant relaxation (Yelda et al. 2014), suggesting that the inclination instability may have expanded the disk. We explore this possibility in future work.

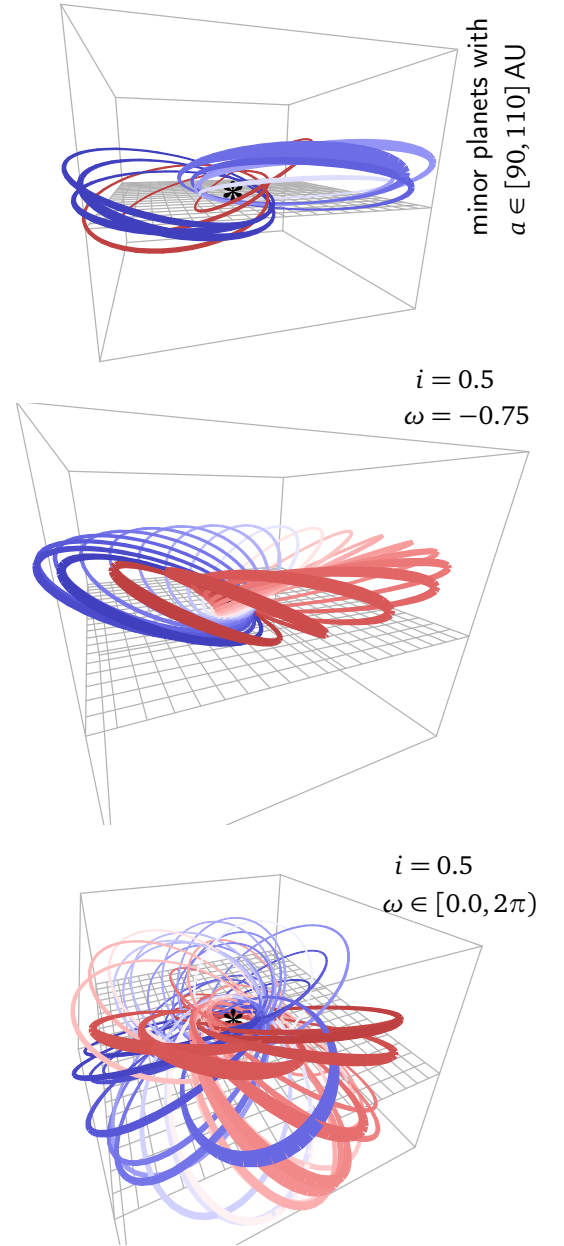


Figure 4. Geometric meaning of “clustering in ω .” (*middle*): a disk of 20 orbits, all with identical semi-major axis a , eccentricity $e = 0.8$, inclination $i = 0.5$, and angle of pericenter $\omega = -0.75$. Longitude of ascending node Ω uniformly fills $[0, 2\pi)$ and is indicated with color. Disks which cluster in ω represent “cones” with the center of mass above or below the disk plane, and with each orbit tilting in the same fashion. (*bottom*): the same disk, but each orbit is given a random value of $\omega \in [0, 2\pi)$; in this (much more generic) case, the disk becomes a thick torus. (*top*): Orbits for minor planets with semi-major axis lengths between 90 and 110 AU; the disk clusters in ω and has a cone-shape as seen in the middle panel. (We restrict the semi-major axis lengths to a narrow range for clarity; the results look similar for other ranges.)

REFERENCES

- Chambers J. E., 1999, MNRAS, 304, 793
Duncan M., Quinn T., Tremaine S., 1987, AJ, 94, 1330
Gladman B., Holman M., Grav T., Kavelaars J., Nicholson P., Aksnes K., Petit J.-M., 2002, Icarus, 157, 269
Gladman B., Kavelaars J. J., Petit J.-M., Morbidelli A., Holman M. J., Loredó T., 2001, AJ, 122, 1051
Hills J. G., 1981, AJ, 86, 1730
Ida S., 1990, Icarus, 88, 129
Lorenzo I., 2007, Monthly Notices of the Royal Astronomical Society, 375, 1311
Madigan A.-M., Levin Y., Hopman C., 2009, ApJ, 697, L44
Rauch K. P., Tremaine S., 1996, New Astronomy, 1, 149
Trujillo C. A., Sheppard S. S., 2014, Nature, 507, 471
Tsiganis K., Gomes R., Morbidelli A., Levison H. F., 2005, Nature, 435, 459
Yelda S., Ghez A. M., Lu J. R., Do T., Meyer L., Morris M. R., Matthews K., 2014, ApJ, 783, 131

Acknowledgements A.-M.M. thanks C. Nixon, M. Jalali, A. Parker, B. Sherwin and F. Van de Voort for helpful conversations. We thank R. Murray-Clay, E. Chiang and E. Quataert for comments on an earlier draft. A.-M.M. was supported by NASA through Einstein Postdoctoral Fellowship Award Number PF2-130095. M.M. was supported by the National Science Foundation (NSF) grant AST-1312651 and NASA grant NNX15AK81G. The authors acknowledge the Texas Advanced Computing Center (TACC) for providing HPC resources that have contributed to the research results reported here. This work used the Extreme Science and Engineering Discovery Environment (XSEDE allocations TG-AST140039, TG-AST140047, and TG-AST140083), which is supported by NSF grant number ACI-1053575. We used the open-source software *toga* to make our plots.